chemosensors

MDPI

Article

Highly Efficient, Non-Covalent Functionalization of CVD-Graphene via Novel Pyrene-Based Supporter Construct

Misbah Shahzadi [1,†], Sobia Nisar [2,†], Deok-Kee Kim [2,*], Nasir Sarwar [3], Aamir Rasheed [4], Waqas Ahmad [5], Amir Muhammad Afzal [6], Muhammad Imran [7], Mohammed Ali Assiri [7], Zafar M. Shahzad [3,5,*] and Ghulam Dastgeer [8,*]

1 Department of Chemistry, University of Agriculture, Faisalabad 38040, Pakistan
2 Department of Electrical Engineering, Sejong University, Seoul 05006, Republic of Korea
3 Department of Textile Engineering, University of Engineering & Technology, Lahore, Faisalabad Campus, Faisalabad 38000, Pakistan
4 Department of Chemistry, University of Ulsan, Ulsan 44610, Republic of Korea
5 Department of Chemical and Polymer Engineering, University of Engineering & Technology, Lahore, Faisalabad Campus, Faisalabad 38000, Pakistan
6 Department of Physics, Riphah International University, Lahore Campus, 13-Km Raiwind Road Lahore, Lahore 54000, Pakistan
7 Department of Chemistry, Faculty of Science, King Khalid University, P.O. Box 9004, Abha 61413, Saudi Arabia
8 Department of Physics and Astronomy, Sejong University, Seoul 05006, Republic of Korea
* Correspondence: deokkeekim@sejong.ac.kr (D.-K.K.); mshahzad@skku.edu (Z.M.S.); gdastgeer@sejong.ac.kr (G.D.)
† These authors contributed equally to this work.

Abstract: Ultra-thin two-dimensional (2D) materials have attained huge interest for biosensing applications because of their strong electrostatic coupling with target molecules such as spike proteins and DNA. One such 2D material is graphene, which is extremely thin and flexible and has a strong non-covalent interaction with the supporting constructs needed to detect biomolecules. This work aimed to develop a way to efficiently functionalize the surface of 2D material using a pyrene-based supporter construct to detect the target protein. For this purpose, high-quality, pristine graphene was grown via the chemical vapor deposition (CVD) method and transferred over the Si/SiO_2 substrate for its functionalization using our engineered pyrene–lysine-based supporter construct (PLB). The construct was synthesized using the solid-phase peptide synthesis (SPPS) method and utilized to functionalize the graphene-channel-based field-effect transistor (FET) device via non-covalent $\pi-\pi$ stacking interaction. The optimum concentration of the functionalized PLB was evaluated via atomic force microscopy (AFM), Raman spectroscopy, and real-time electrical measurements. The characterization techniques successfully provide an overview of the effect of the concentration of PLB used for functionalization. Moreover, the performance was tested and compared in terms of the percentage response of the device generated after the detection of various concentrations of the streptavidin protein. This research could be useful in determining how to functionalize any 2D material by designing a supporter construct without material degradation and owing to over-stacking or bypassing surface screening effects.

Keywords: protein; graphene FET; device functionalization; biosensing

check for updates

Citation: Shahzadi, M.; Nisar, S.; Kim, D.-K.; Sarwar, N.; Rasheed, A.; Ahmad, W.; Afzal, A.M.; Imran, M.; Assiri, M.A.; Shahzad, Z.M.; et al. Highly Efficient, Non-Covalent Functionalization of CVD-Graphene via Novel Pyrene-Based Supporter Construct. *Chemosensors* **2023**, *11*, 83. https://doi.org/10.3390/chemosensors11020083

Academic Editor: Xiaolong Yang

Received: 27 December 2022
Revised: 17 January 2023
Accepted: 19 January 2023
Published: 21 January 2023

Copyright: © 2023 by the authors. Licensee MDPI, Basel, Switzerland. This article is an open access article distributed under the terms and conditions of the Creative Commons Attribution (CC BY) license (https://creativecommons.org/licenses/by/4.0/).

1. Introduction

Two-dimensional materials such as graphene are being functionalized through various routes to explore their structural and morphological features for utilization in catalysis, energy-harvesting materials, and biosensing [1–5]. The biosensors based on graphene or semiconductor 2D materials can sense surface changes from their surroundings and offer the best sensing environment for ultrasensitive and low-noise detection.

This makes graphene-based FET technology extremely appealing for uses involving delicate immunological diagnostics. As a matter of fact, covalent functionalization constitutes the sp^2 structure of graphene lattices, thus resulting in defects and loss of the electronic properties during functionalization [1,6]. In contrast, non-covalent functionalization is largely preferred as it does not alter the structure and electronic properties of graphene while inducing new groups onto the surface, possibly due to forces such as $\pi-\pi$ interactions, hydrogen bonding, and van der Waals forces. Hence, it leads to enhanced dispersibility, biocompatibility, reactivity, binding capacity, and sensing properties [7–11]. However, the main challenge in functionalizing graphene and graphene-like material is determining the optimum concentration of the receptor so as to avoid the loss of material due to over-stacking and also avoiding various screening effects, such as Debye screening length. [12–15] We tried to cover this gap by engineering a short-peptide-containing pyrene moiety and utilizing it for the functionalization of CVD-grown good-quality pristine graphene. For the fabrication of the graphene-based FET biosensor, the p-doped silicon substrates were coated with 300 nm thick silicon oxide (SiO_2) and washed with acetone and isopropanol and dried with nitrogen gas (N_2) to ensure absolute cleanliness. The CVD-grown graphene was transferred onto our working substrate (Si/SiO_2) and analyzed under Raman spectroscopy to analyze the properties of graphene after its functionalization using various concentrations of our PLB construct. Our engineered construct had a pyrene molecule at the terminal end so that it could make stable $\pi-\pi$ stacking interactions with the hexagonal structure of graphene rings. Pyrene has a larger number of free electrons as compared to graphene. Hence, it shared its free electrons with the graphene and made non-covalent ($\pi-\pi$) bonding interactions, as shown in Figure 1a. This study is backed by the AFM measurements of the height profile of the substrate before and after functionalization. In addition to the above, we patterned the electrodes using photolithography and a thermal metal deposition chamber on the same substate and fabricated a back-gated FET device for detailed electrical characterization. The 1 nM concentration was found to be ideal for channel functionalization with our designed construct of PLB.

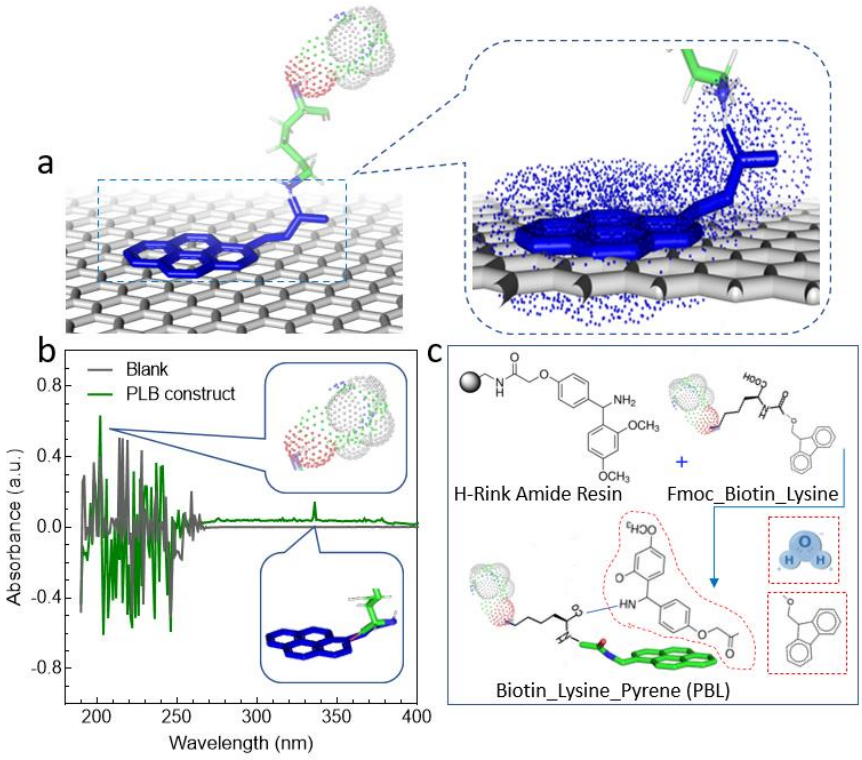


Figure 1. A schematic demonstration of functionalizing graphene with our engineered pyrene-based construct. (**a**) Pyrene interacts with graphene rings by sharing its free electrons. (**b**) The synthesized

PLB construct was tested (via middle/long-wave UV spectra) for the successful conjugation of pyrene and the presence of biotin. Sharp clear peaks at 202 nm and 335 nm confirm the presence of biotin and pyrene. (**c**) The reaction mechanism for our engineered PLB construct. The synthesis reaction constitutes a series of deprotection and coupling steps. The Fmoc was removed via deprotection using piperidine while coupling was assisted by coupling solution containing DIC and Oxyma.

2. Material and Methods

2.1. The Growth of High-Quality Pristine Graphene (PG)

Usually, substrates are functionalized using various two-dimensional (2D) materials [16–19], and their properties, which reflect various binding events, are monitored. In this regard, a 2D sp2-bonded carbon allotrope, graphene, has attracted enormous interest over the past decade due to its unique properties, such as ultrahigh electron mobility, uniform broadband optical absorption, and high tensile strength. Hence, monolayer, large-size, and high-quality pristine graphene was grown via the chemical vapor deposition (CVD) method. This method was selected since CVD-derived graphene is polycrystalline and good-quality [20–23]. The copper-foil nook was shaped by twisting a 25 mm thick copper foil (Nilaco Corporation, Tokyo, Nilaco Bldg., Japan) and afterward creasing the three leftover sides. Methane flow was kept at 1 sccm at 50 mTorr, and the temperature remained at 1035 °C followed by the 2.0 h ramping process. At temperatures above 1035 °C, large-domain graphene growth was observed on the copper-foil enclosure. The procedure is described in agreement with the literature [24–28].

Graphene grew on both the inside and outside of the Cu enclosure. The back-end graphene was etched via oxygen plasma etching. The graphene was coated with PMMA using a spin coater at 4000 PRM for 1 min. After transferring, the Si/SiO_2 substrate was dried in an oven at 80 °C for 1 h Finally, the substrate was dried by a nitrogen blow followed by washing using acetone for PMMA removal and methanol for acetone removal. The graphene layer was transferred to our working substrate (Si/SiO_2) via the wet transfer method, using iron (III) chloride as an etchant. The transferred monolayer graphene was characterized using Raman spectra analysis, showing an excellent 2D/G ratio with a negligible defect peak, as shown in Figure 2a.

2.2. The Device Fabrication for Electrical Measurements

After transferring the CVD-grown graphene over the Si/SiO_2 substrates, the substrates were coated with polymers of EL-9 and photoresist (PR) and baked over the hot plate at 170 °C and 100 °C, respectively. The photolithography technique was utilized to draw the electrode pattern over the graphene. After photolithography, all the substrates were loaded in the thermal evaporator chamber for the deposition of the Cr/Au electrodes. In a high vacuum of 5×10^{-6} torr, 5 nm thick Cr and 50 nm thick gold films were deposed to draw the source–drain electrodes. After metal deposition, the substrates were washed with acetone and methanol for the liftoff process and dried with N_2. In order to measure the electrical properties of the device, these source and drain electrodes were used to apply biasing voltage and measure the output current, respectively. After the deposition of electrodes, the final devices were annealed at 200 °C for 2.0 h under a suitable pressure, in the presence of argon. The electrical properties of our graphene-channel-based field-effect transistor were measured using a three-probe station. The inner probes were connected to a voltage meter, while the two outer probes were connected to source and drain electrodes drawn over the graphene channel. The gate voltage and biasing voltages were controlled via a source meter (Keitley K-2400), and the output current was recorded using a pico-ammeter (Keithley K-6485). The voltage drop across the inner probes was measured as current flowed between the outer probes. All the electrical and real-time measurements were performed in the ambient environment and at room temperature. The resistivity of the material being tested determines how the current and voltage values relate to one another.

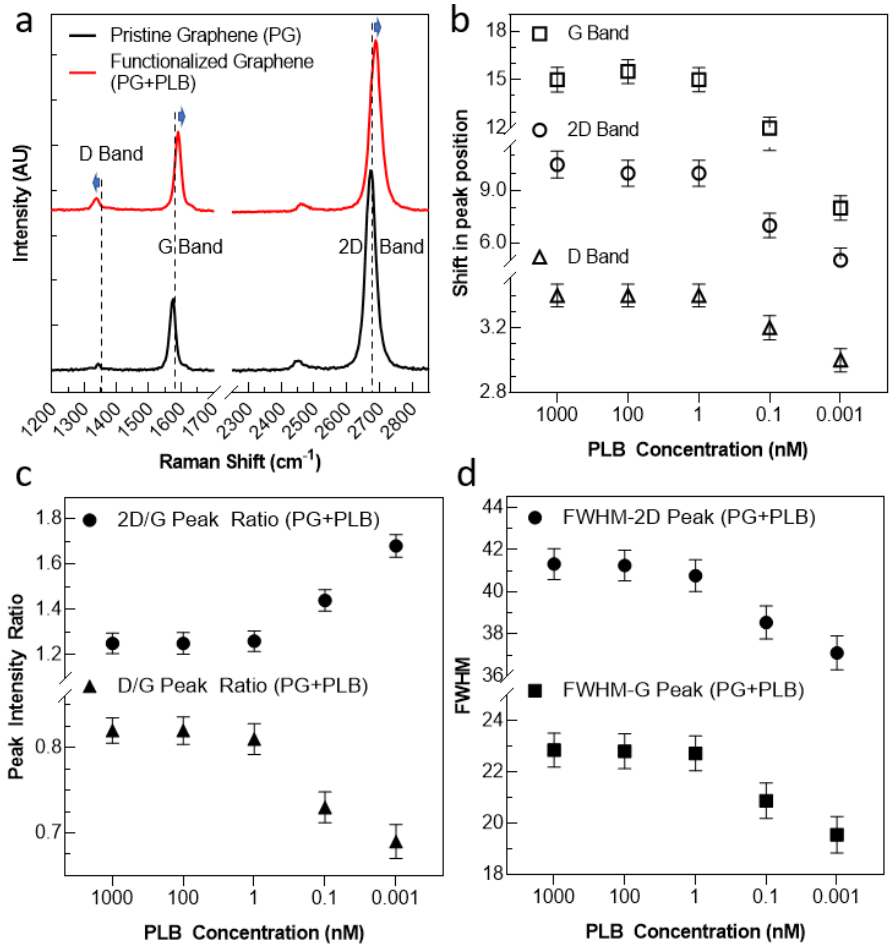


Figure 2. The Raman spectra analysis of our substrate before and after functionalization using various PLB concentrations. (**a**) Pyrene interacts with graphene rings by sharing its free electrons. (**b**) The synthesized PLB construct was tested (via middle/long-wave UV. (**c**) The peak ratios were plotted as a function of PLB molecule concentration. (**d**) The FWHM for 2D peak and G peak are illustrated as a function of PLB molecule concentration.

2.3. The PLB Synthesis

In this work, we utilized a self-engineered pyrene–lysine–biotin (PLB) construct for the functionalization of our substrate material (graphene). Using Fmoc chemistry-based H-Rink amide resin, a manual solid-phase peptide synthesizer (SPPS) was used to synthesize the PLB construct. The resin, because of the 0.14 mmol synthesis scale, was expanded in DMF for 30 min and deprotected utilizing 20% piperidine in N,N-dimethylformamide at 90 °C ± 5 for 50 s followed by 75 °C ± 5 for 15 s. The principal wash was conducted with DMF and the secondary was carried out using dichloromethane in between each deprotecting and coupling step. For synthesis, 0.2 M Fmoc-Lys (Biotin) (prepared according to provider protocol) was added to activated amino acid (DIPEA), using DMF as a solvent in the presence of 0.5 M DIC and 1 M Oxyma at 90 °C ± 5 for 110 s followed by 75 °C ± 5 for 15 s. Repeating the deprotection step, the 1-pyrene butyric acid was used for the coupling reaction in the circumstances referenced previously. The finished product was dried for 1 h in a desiccator. Using a trifluoroacetic-acid-containing cleavage solution, the product was cleaved from the solid support and was achieved by mixing it with triisopropylsilane (2.5%) and water (2.5%) at room temperature for 2 h. The confirmation of coupling and deprotection was made at each phase using the ninhydrin test. A schematic of this reaction is presented in Figure 1c. Before utilizing this construct for functionalization, the presence of pyrene was confirmed by measuring absorbance at 335 nm, as shown in Figure 1b.

3. Results and Discussion

In our experimental investigation, a pyrene-based construct was engineered and used to functionalize high-quality pristine graphene. In order to find out the best conditions of functionalization, avoiding over-stacking and loss of material, solutions (with the PLB construct) with various concentration were prepared and drop-cast to functionalize the channel material. After washing and drying, the final graphene-based FET device was characterized using various techniques, such as Raman spectra, AFM, and electrical measurements, and the results are presented below.

3.1. The Raman Spectra Analysis

To evaluate the efficiency of functionalization and find the optimum concentration for functionalization, the substrate, containing various concentrations of PLB, was drop-cased and washed–dried for analysis. The substrate was subjected to Raman spectroscopy (under 532 nm excitation) to ensure the quality of graphene and assembly of our PLB onto the graphene surface. As the first step, the Raman spectra of bare graphene were recorded. Two clear peaks (G and 2D peaks) were observed (black line in Figure 2a). The G peak corresponds to the lattice vibration mode, and the 2D peak stems from second-order Raman scattering. There was no D peak seen corresponding to any defects while transferring graphene to the Si/SiO_2 substrate. After confirming the presence of defect-free pristine graphene, we functionalized the channel using our PLB construct. In spectra (red line in Figure 2a), a clear right shift in the G peak and 2D peak position can be seen, which indicates p-doping by the $\pi-\pi$ interaction between the pyrene molecule and graphene. To further validate this observation, we measured the spectra at various devices and plotted the peak positions, as shown in Supplementary Figure S1, to confirm this shifting upon functionalization. Moreover, the layer-dependent ratio of the intensity of the 2D band to the G band (2D/G) fell from 1.71 to 1.26, as shown in Supplementary Figure S2a. Adding to this, a D peak (at ~1342 cm^{-1}) was also observed and shifted downwards upon functionalization. This D peak appears to be due to the introduction of disorder arising from the orbital hybridization of the molecule with the graphene plane [29–31]. Further, an increase in FWHM in the G and 2D peaks can be seen, depicting the loss in crystallinity of graphene on the surface after its functionalization, as shown in Supplementary Figure S2b.

Further, the Raman spectra peak property analysis was carried out by varying the concentration of the PLB construct from 0.001 nM to 1000 nM, as shown in Figure 2b–d. From the peak property analysis, a clear shift in all peak positions can be seen from concentrations of 0.001 nM to 1 nM, whereas a marginal shift in peak position was observed upon the further increase in PLB concentration, indicating the saturation of the surface at ~1 nM PLB. The trend seems consistent with all the peak positions (Figure 2b). In order to validate the data, the testing was performed using three different substrates (N = 3), and its mean was plotted along with the standard deviation to avoid errors in measurement. Moreover, a similar leveling off of variation trend was observed with the peak intensity ratio (Figure 2c) and FWHM of the main and second resonance peaks (Figure 2d). Hence, through the Raman spectra investigation, a concentration of around 1 nM of our PLB construct was considered sufficient to fully functionalize the substrate, without causing unwanted doping and loss of material.

3.2. The AFM Analysis

Furthermore, the substrate was analyzed using atomic force microscope (AFM, I-Nexus Co., Ltd., Seoul, Republic of Korea) measurements to investigate surface conditions. Since the capacitance (*C*) of a graphene FET is inversely proportional to the distance (d) between the graphene and the charged biomolecule, the thickness of the receptor is an important parameter for determining the electrostatic coupling strength between the graphene and the charged biomolecules, when the graphene is functionalized.

$$C = \frac{\alpha \beta A}{d} \quad (1)$$

where C is the capacitance, β is the absolute permittivity, d is the thickness of the PLB construct (receptor), A is the area of the graphene channel, and α is the relative permittivity.

Hence, the graphene surface was functionalized with a buffer solution containing various concentrations of PLB to confirm the effect of the receptor thickness on the graphene biosensor. The self-assembled PLB construct's AFM profile on the graphene surface at various concentrations is depicted in Figure 3. For the self-assembly property study, the lyophilized powder of pure PLB was dissolved in distilled water, Tris buffer (20 mM), and NaCl (5 mM) to create solutions of 0.001 nM, 100 nM, and 1000 nM. Both the procedure and the buffer were chosen in accordance with the literature. Before the AFM analysis, the substrate was triple-washed with the same buffer and dried. Based on the interaction, the pyrene residue of the PLB construct interacted with graphene, enabling the construct to be uniformly assembled on the graphene surface without leaving any voids. The substrate with a high concentration of PLB showed stacking of material after the surface saturated, as shown in Figure 3c,d. It can be observed that the average height of the surface containing bare graphene was ~0.4 nm while the height increased up to ~1.5 nm upon functionalization with the PLB construct, which can be attributed to the formation of a monolayer PLB construct on the graphene surface. Moreover, it can be observed that, when using a low concentration of PLB (0.001 nM, Figure 3a), there were a lot of empty spaces still vacant for functionalization. However, after increasing the concentration to 1 nM, most of the surfaces became occupied, leaving fewer vacant positions, Figure 3b. It is noteworthy that by further increasing PLB concentration, the height increased, forming rough lumps without an ordered orientation, which indicated clear stacking of material onto the surface, as seen in Figure 3d.

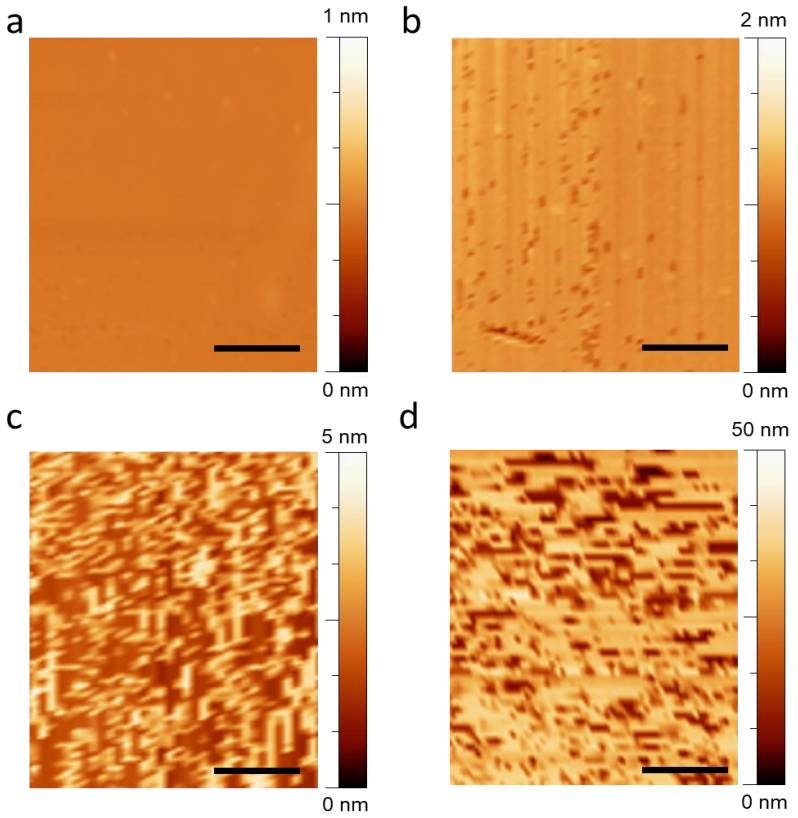


Figure 3. The atomic force microscopic image of our graphene channel substrate after functionalizing using PLB construct at increasing concentrations. (**a**) The AFM image of graphene surface containing 0.001 nM PLB construct for functionalization. (**b**–**d**) The AFM image of graphene-channel-based substrate with 1 nM, 100 nM, and 1000 nM PLB, respectively. The inset scale bar in each figure is equivalent to 2 μm.

3.3. The Electrical Measurements

To further validate the results, we made an FET device by impeding source and drain electrodes and subjected the device to detailed electrical measurements (see Figures S3 and S4). The linear I_{DS}-V_{DS} curves at zero gate voltage are presented in Figure 4a, exhibiting the drain characteristics of the device after functionalization. Initially, the pristine graphene FET was measured without any treatment of the PLB molecules by increasing the source–drain voltage from −2 V to 2V. In pristine condition (black line in Figure 4a), a straight line passing through the origin means the device has ohmic behavior. It can be observed that the output current started to rise after increasing the concentration of the PLB supporter construct over the graphene surface. Further, after functionalizing with a higher concentration of PLB, a dominant increase in current was observed, saturating at ~1 nM PLB concentration. This saturation in current shows a reasonable functionalization of the graphene surface. Further, the transfer curves of the graphene FET were measured by increasing the back gate voltage from −30 to 30 V. A sufficient variation in Dirac point voltage can also be observed before and after functionalization of the graphene FET, as shown in Figure 4b. For the pristine graphene, the Dirac point existed at zero voltage, which shifted to around 10 V after functionalization with the PLB. The scanning electron microscopeic (SEM) image of the final device is illustrated in the Figure 4b inset. All the measurements were conducted using three different devices, and the mean/standard deviation is plotted in Figure 4c,d.

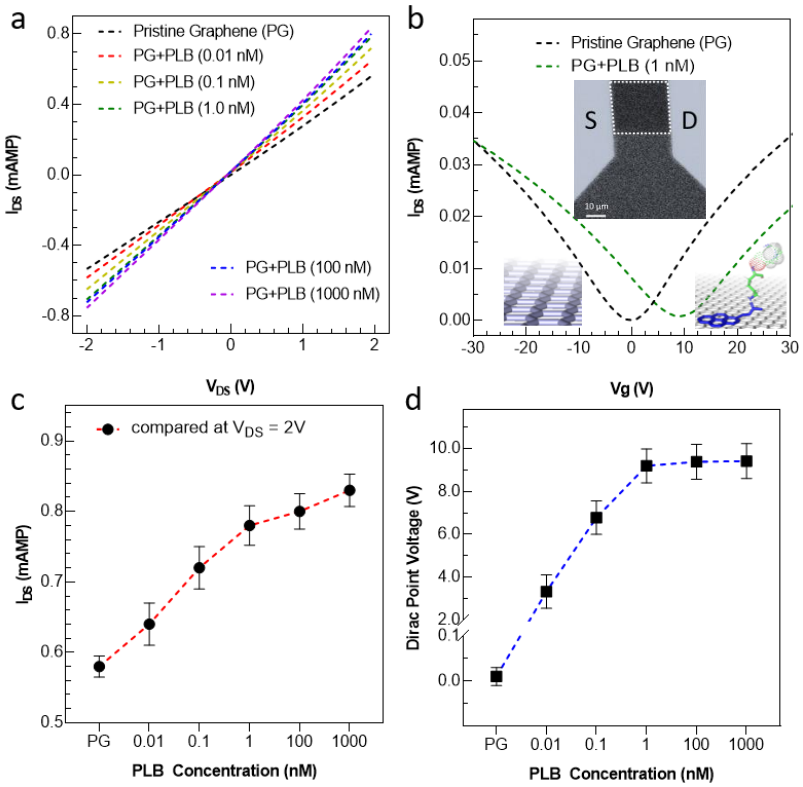


Figure 4. Electrical property analysis of the device before and after functionalizing with our PLB construct at various concentrations. (**a**) The output characteristics (at V_g = 0 V) of the device before and after functionalization. The current increases upon functionalization due to transfer of free electrons from pyrene to graphene. (**b**) The transfer characteristic of the device before and after functionalization. The Dirac point lies around 0 V, showing perfect growth and transfer procedure without any serious external doping. After functionalization, a clear shift in DIRAC point voltage was observed, owing to the p-doping of graphene upon functionalization. The SEM image of the final graphene FET device is shown in the inset with a scale bar of 10 µm. The white dotted rectangular region shows the graphene channel area. (**c**,**d**) A relative increase in current at (V_{DS} = 2 V) and Dirac point voltage V_{DS} = 0.01 V) was achieved by increasing the concentration of PLB.

3.4. The Real-Time Response

In testing the performance of the device in real time, a reduction in the current (I_{DS}) from its baseline was noted (for three different devices) concerning time, as seen Figure 5. For a comparison without error, the normalized level of current was calculated using Equation (2).

$$Normalized\ I_{DS} = \frac{I - Io}{Io} \quad (2)$$

where I is the current at any time (t) while Io is the current at the time (t = 0). The real-time electrical measurements were performed at a steady bias voltage of 0.01 V. Three different devices with uncovered graphene channels were equilibrated with buffer, and their ongoing current profiles with PLB-covered graphene channels of various concentrations (0.001 nM (red line), 1 nM (green line), and 100 nM (blue line)) are presented in Figure 5a. None of the devices showed any considerable current change during buffer application, so we accepted this as a baseline for functionalization. When the solution containing 0.01 nM PLB was drop-cast onto the channel, the level of current increased but the trend leveled off within a short time of 2 min. This short time of functionalization is due to the perfection of our engineered construct, which is free from any kind of surface screening effects and other issues, such as steric hindrance. After the current was maintained, the device was washed using the same buffer, and the level of current remained the same before and after washing, as shown in Figure 5a (in red line). To improve the level of current, we increased the PLB concentration to 1 nM with the second device and noted the current profile. It was observed that the level of current improved, and after washing, a negligible drop in current was observed, as shown in Figure 5a (green line). However, when we further increased the PLB concentration on our third device, the level of current improved a little bit, and after washing, it dropped sharply, indicating the stacking of PLB molecules due to saturation of the sensor surface at that high concentration (100 nM), as shown in Figure 5a (blue line). All the real-time measurements were repeated using three different devices, and the results are presented in Figure 5b. Since our construct was biotinylated and its presence was confirmed using middle/long-wave UV spectra (Figure 1b), the device was subjected to a solution containing streptavidin. The source–drain current decreased after the streptavidin addition because some of the PLB molecules' charges were occupied by streptavidin molecules. As a result, a small number of charges were transferred from the PLB to the graphene surface, which caused a decrease in current [5,9,10]. The time in which device current is saturated after capturing the streptavidin is known as the response time. The real-time measurements exhibited that our device current was saturated within ~30 s after adding the target protein (streptavidin) solution, which means that graphene devices can successfully detect the target protein (streptavidin) within ~30 s, as shown in Figure 5c. The comparison of the graphene FET with other biosensor devices is illustrated in Figure S5. It is worth noting that the level of current after streptavidin application and adding another washing step (washing-2) was almost the same. Moreover, the specificity of the device was tested by applying a similar concentration of nearly similar molecular weight protein, i.e., bovine serum albumin (BSA), which gave no considerable response as compared to the target protein (see Figure S6). Followed by initial trials of concentration, a fixed concentration of 1 nM streptavidin was used to compare the devices functionalized using three various concentrations of the PLB construct, the results of which are presented in Figure 5d.

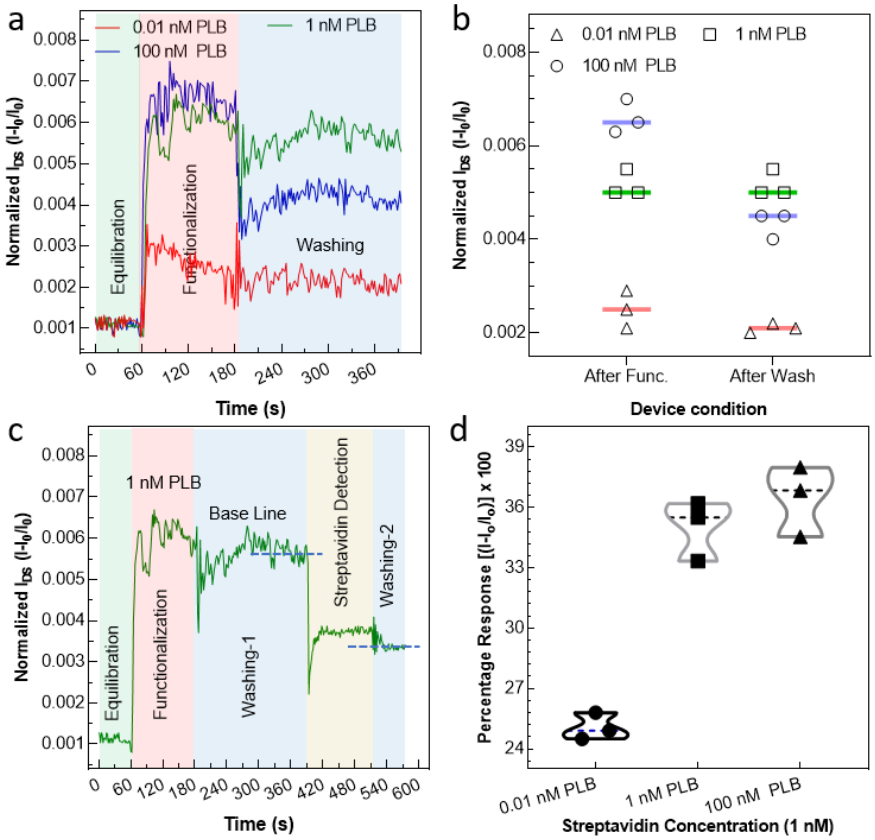


Figure 5. Real-time electrical measurement of the G-FET device. (**a**) The current profile of the device after applying PLB at various concentrations ranging from 0.01 nM to 100 nM. After the current became constant, washing was carried out using the same buffer to get rid of the PLB molecules stacked onto the surface with bonds other than the graphene surface. (**b**) The normalized current for three different devices was measured right after functionalization and after applying the washing step. The experimental investigation revealed that the 1 nM PLB concentration was adequate to functionalize all the graphene channel surfaces, avoiding any surface screening and loss of material due to stacking. (**c**) Finally, the same device was used to detect the streptavidin, since the PLB construct was biotinylated. (**d**) The graph was plotted to observe the percentage response of devices functionalized using various concentrations of PLB. For all the measurements, the concentration of streptavidin was kept constant. The optimum response, i.e., obtaining a max response without wasting material (PLB), was obtained at 1 nM PLB.

4. Conclusions

In this work, we demonstrated a way to efficiently functionalize (non-covalently) a graphene-channel-based field-effect transistor using our self-engineered pyrene-based supporter construct (PLB). The monomolecular self-assembly of our peptide construct was made possible due to $\pi-\pi$ stacking of free electrons with graphene's Bravais lattice, allowing ultra-thin monomolecular self-assembly via the graphene lattice. It is worth mentioning that functionalizing 2D materials, especially graphene, is not new; however, we demonstrated a way to achieve an ultra-thin receptor using our engineered construct, which enabled high gate coupling between the PLB construct and graphene channel. The thickness profile was measured and analyzed via various routes, such as Raman spectra, AFM, and electrical measurements. Owing to our novel PLB construct and efficient way to screen out the desired concentration for efficient functionalization, our device demonstrated excellent results in real time, and a prompt inherent response was observed. For the practical application of the device as a biosensor, streptavidin protein was also detected using the graphene-based FET after exploring the functionalization technique. Our developed strategy can help in evaluating the best way to functionalize any 2D material surface

efficiently with good surface density, avoiding any degradation [9] of material and surface screening effects.

Supplementary Materials: The following supporting information can be downloaded at: https://www.mdpi.com/article/10.3390/chemosensors11020083/s1, Figure S1: The Raman spectra peak position analysis of graphene-based substrate before and after functionalization; Figure S2: The Raman spectra analysis of graphene-based substrate before and after functionalization. (a) The analysis of intensity ratio of main, second resonance, and defect peak before and after functionalization. (b) The FWHM of the peak before and after functionalization. All the data were plotted using N = 3 to eliminate possible variation in the marked value; Figure S3: The optical image of graphene on Si/SiO_2 substrate, confirming unbroken graphene layer transfer via wet transfer method; Figure S4: The sketch of our device for electrical measurements, created using CREO 6.0; Figure S5: The comparison of results for streptavidin detection of our device; Figure S6: A comparison of streptavidin and bovine serum albumin (BSA) at various concentrations is plotted with error bars with an accuracy of 95%.

Author Contributions: G.D., S.N., M.S. and Z.M.S. designed the project M.S. and S.N. performed the experimental work. G.D., D.-K.K. and Z.M.S. supervised the project and wrote the final manuscript. N.S., W.A., A.M.A., A.R., M.I. and M.A.A. analyzed the data and reviewed the manuscript. All the authors reviewed and revised the final manuscript. M.S. and S.N. share 1st authorship equally. All authors have read and agreed to the published version of the manuscript.

Funding: This research was funded by the National Research Foundation (2022R1G1A1009887), Korea, and Sejong University, Seoul 05006, Korea.

Data Availability Statement: The data presented in this study are available on request from the corresponding authors.

Acknowledgments: This research was funded by the National Research Foundation (2022R1G1A1009887), Korea, and Sejong University, Seoul 05006, Korea, and all the authors are thankful for this support. M.A.A. extends their appreciation to the Ministry of Education in KSA for funding this research work through project number KKU-IFP2-DA-1.

Conflicts of Interest: The authors declare no conflict of interest.

References

1. Georgakilas, V.; Tiwari, J.N.; Kemp, K.C.; Perman, J.A.; Bourlinos, A.B.; Kim, K.S.; Zboril, R.J. Noncovalent functionalization of graphene and graphene oxide for energy materials, biosensing, catalytic, and biomedical applications. *Chem. Rev.* **2016**, *116*, 5464–5519. [CrossRef] [PubMed]
2. Su, Q.; Pang, S.; Alijani, V.; Li, C.; Feng, X.; Müllen, K.J. Composites of graphene with large aromatic molecules. *Adv. Mater.* **2009**, *21*, 3191–3195. [CrossRef]
3. Kim, J.; Song, S.H.; Im, H.G.; Yoon, G.; Lee, D.; Choi, C.; Kim, J.; Bae, B.S.; Kang, K.; Jeon, S. Moisture barrier composites made of non-oxidized graphene flakes. *Small* **2015**, *11*, 3124–3129. [CrossRef] [PubMed]
4. Forsyth, R.; Devadoss, A.; Guy, O.J. Graphene field effect transistors for biomedical applications: Current status and future prospects. *Diagnostics* **2017**, *7*, 45. [CrossRef] [PubMed]
5. Zafar, M.S.; Dastgeer, G.; Kalam, A.; Al-Sehemi, A.G.; Imran, M.; Kim, Y.H.; Chae, H. Precise and Prompt Analyte Detection via Ordered Orientation of Receptor in WSe2-Based Field Effect Transistor. *Nanomaterials* **2022**, *12*, 1305. [CrossRef] [PubMed]
6. Kim, J.E.; No, Y.H.; Kim, J.N.; Shin, Y.S.; Kang, W.T.; Kim, Y.R.; Kim, K.N.; Kim, Y.H.; Yu, W.J. Highly sensitive graphene biosensor by monomolecular self-assembly of receptors on graphene surface. *Appl. Phys. Lett.* **2017**, *110*, 203702. [CrossRef]
7. MacLeod, J.; Lipton-Duffin, J.; Cui, D.; De Feyter, S.; Rosei, F. Substrate effects in the supramolecular assembly of 1, 3, 5-benzene tricarboxylic acid on graphite and graphene. *Langmuir* **2015**, *31*, 7016–7024. [CrossRef]
8. Stradi, D.; Garnica, M.; Díaz, C.; Calleja, F.; Barja, S.; Martín, N.; Alcamí, M.; de Parga, A.L.V.; Miranda, R.; Martín, F. Controlling the spatial arrangement of organic magnetic anions adsorbed on epitaxial graphene on Ru (0001). *Nanoscale* **2014**, *6*, 15271–15279. [CrossRef]
9. Seo, G.; Lee, G.; Kim, M.J.; Baek, S.-H.; Choi, M.; Ku, K.B.; Lee, C.-S.; Jun, S.; Park, D.; Kim, H.G.; et al. Rapid Detection of COVID-19 Causative Virus (SARS-CoV-2) in Human Nasopharyngeal Swab Specimens Using Field-Effect Transistor-Based Biosensor. *ACS Nano* **2020**, *14*, 5135–5142. [CrossRef]
10. Fathi-Hafshejani, P.; Azam, N.; Wang, L.; Kuroda, M.A.; Hamilton, M.C.; Hasim, S.; Mahjouri-Samani, M. Two-Dimensional-Material-Based Field-Effect Transistor Biosensor for Detecting COVID-19 Virus (SARS-CoV-2). *ACS Nano* **2021**, *15*, 11461–11469. [CrossRef]

11. Zhang, X.; Liu, T.; Boyle, A.; Bahreman, A.; Bao, L.; Jing, Q.; Xue, H.; Kieltyka, R.; Kros, A.; Schneider, G.F.; et al. Dielectric-Modulated Biosensing with Ultrahigh-Frequency-Operated Graphene Field-Effect Transistors. *Adv. Mater.* **2022**, *34*, 2106666. [CrossRef] [PubMed]
12. Nakatsuka, N.; Yang, K.-A.; Abendroth, J.M.; Cheung, K.M.; Xu, X.; Yang, H.; Zhao, C.; Zhu, B.; Rim, Y.S.; Yang, Y.; et al. Aptamer–field-effect transistors overcome Debye length limitations for small-molecule sensing. *Science* **2018**, *362*, 319–324. [CrossRef] [PubMed]
13. Huang, W.; Diallo, A.K.; Dailey, J.L.; Besar, K.; Katz, H.E. Electrochemical processes and mechanistic aspects of field-effect sensors for biomolecules. *J. Mater. Chem. C Mater.* **2015**, *3*, 6445–6470. [CrossRef] [PubMed]
14. Dastgeer, G.; Nisar, S.; Shahzad, Z.M.; Rasheed, A.; Kim, D.-K.; Jaffery, S.H.A.; Wang, L.; Usman, M.; Eom, J. Low-Power Negative-Differential-Resistance Device for Sensing the Selective Protein via Supporter Molecule Engineering. *Adv. Sci.* **2022**, *10*, 2204779. [CrossRef] [PubMed]
15. Dastgeer, G.; Shahzad, Z.M.; Chae, H.; Kim, Y.H.; Ko, B.M.; Eom, J. Bipolar Junction Transistor Exhibiting Excellent Output Characteristics with a Prompt Response against the Selective Protein. *Adv. Funct. Mater.* **2022**, *32*, 2204781. [CrossRef]
16. Jeong, J.H.; Kang, S.; Kim, N.; Joshi, R.K.; Lee, G.-H. Recent trends in covalent functionalization of 2D materials. *Phys. Chem. Chem. Phys.* **2022**, *24*, 10684–10711. [CrossRef] [PubMed]
17. Amieva, E.J.C.; López-Barroso, J.; Martínez-Hernández, A.L.; Velasco-Santos, C. Graphene-based materials functionalization with natural polymeric biomolecules. *Recent Adv. Graphene Res.* **2016**, *1*, 257–298.
18. Xie, T.; Liu, Y.; Xie, J.; Luo, Y.; Mao, K.; Huang, C.; Li, Y.; Zhen, S. Catalyzed Hairpin Assembly-Assisted DNA Dendrimer Enhanced Fluorescence Anisotropy for MicroRNA Detection. *Chemosensors* **2022**, *10*, 501. [CrossRef]
19. Ameku, W.A.; Negahdary, M.; Lima, I.S.; Santos, B.G.; Oliveira, T.G.; Paixão, T.R.L.C.; Angnes, L. Laser-Scribed Graphene-Based Electrochemical Sensors: A Review. *Chemosensors* **2022**, *10*, 505. [CrossRef]
20. Li, X.; Cai, W.; Colombo, L.; Ruoff, R.S. Evolution of graphene growth on Ni and Cu by carbon isotope labeling. *Nano Lett.* **2009**, *9*, 4268–4272. [CrossRef]
21. Li, X.; Magnuson, C.W.; Venugopal, A.; An, J.; Suk, J.W.; Han, B.; Borysiak, M.; Cai, W.; Velamakanni, A.; Zhu, Y.; et al. Graphene films with large domain size by a two-step chemical vapor deposition process. *Nano Lett.* **2010**, *10*, 4328–4334. [CrossRef] [PubMed]
22. Deokar, G.; Avila, J.; Razado-Colambo, I.; Codron, J.-L.; Boyaval, C.; Galopin, E.; Asensio, M.-C.; Vignaud, D. Towards high quality CVD graphene growth and transfer. *Carbon* **2015**, *89*, 82–92. [CrossRef]
23. Deng, B.; Liu, Z.; Peng, H. Toward mass production of CVD graphene films. *Adv. Mater.* **2019**, *31*, 1800996. [CrossRef] [PubMed]
24. Li, X.; Magnuson, C.W.; Venugopal, A.; Tromp, R.M.; Hannon, J.B.; Vogel, E.M.; Colombo, L.; Ruoff, R.S. Large-area graphene single crystals grown by low-pressure chemical vapor deposition of methane on copper. *J. Am. Chem. Soc.* **2011**, *133*, 2816–2819. [CrossRef]
25. Yan, Z.; Peng, Z.; Tour, J.M. Chemical vapor deposition of graphene single crystals. *Acc. Chem. Res.* **2014**, *47*, 1327–1337. [CrossRef]
26. Gao, L.; Ren, W.; Zhao, J.; Ma, L.-P.; Chen, Z.; Cheng, H.-M. Efficient growth of high-quality graphene films on Cu foils by ambient pressure chemical vapor deposition. *Appl. Phys. Lett.* **2010**, *97*, 183109. [CrossRef]
27. Wang, C.; Chen, W.; Han, C.; Wang, G.; Tang, B.; Tang, C.; Wang, Y.; Zou, W.; Chen, W.; Zhang, X.-A.; et al. Growth of Millimeter-Size Single Crystal Graphene on Cu Foils by Circumfluence Chemical Vapor Deposition. *Sci. Rep.* **2014**, *4*, 4537. [CrossRef]
28. Yang, Q.; Zhang, Z.; Zhu, W.; Wang, G. Growth of Large-Area High-Quality Graphene on Different Types of Copper Foil Preannealed under Positive Pressure H2 Ambience. *ACS Omega* **2019**, *4*, 5165–5171. [CrossRef]
29. Xu, S.; Zhan, J.; Man, B.; Jiang, S.; Yue, W.; Gao, S.; Guo, C.; Liu, H.; Li, Z.; Wang, J.; et al. Real-time reliable determination of binding kinetics of DNA hybridization using a multi-channel graphene biosensor. *Nat. Commun.* **2017**, *8*, 14902. [CrossRef]
30. Yang, Y.; Asiri, A.M.; Tang, Z.; Du, D.; Lin, Y. Graphene based materials for biomedical applications. *Mater. Today* **2013**, *16*, 365–373. [CrossRef]
31. Wang, X.; Hao, Z.; Olsen, T.R.; Zhang, W.; Lin, Q. Measurements of aptamer–protein binding kinetics using graphene field-effect transistors. *Nanoscale* **2019**, *11*, 12573–12581. [CrossRef] [PubMed]

Disclaimer/Publisher's Note: The statements, opinions and data contained in all publications are solely those of the individual author(s) and contributor(s) and not of MDPI and/or the editor(s). MDPI and/or the editor(s) disclaim responsibility for any injury to people or property resulting from any ideas, methods, instructions or products referred to in the content.